Pacific Northwest
NATIONAL LABORATORY

PNNL- 33314

Noble Gas Management: SBMOF-1 vs. NUCON Carbon

September 2022

Praveen K. Thallapally
Alexander J. Robinson
Ali Zbib
Brian J. Riley
Saehwa Chong
Jian Liu
Mark K. Murphy
Parker Okabe (Flibe Energy)
Roman Sherrod (Flibe Energy)

U.S. DEPARTMENT OF ENERGY

Prepared for the U.S. Department of Energy
under Contract DE-AC05-76RL01830

DISCLAIMER

PACIFIC NORTHWEST NATIONAL LABORATORY
operated by
BATTELLE
for the
UNITED STATES DEPARTMENT OF ENERGY
under Contract DE-AC05-76RL01830

Printed in the United States of America

Available to DOE and DOE contractors from the
Office of Scientific and Technical Information,
P.O. Box 62, Oak Ridge, TN 37831-0062;
ph: (865) 576-8401
fax: (865) 576-5728
email: reports@adonis.osti.gov

Available to the public from the National Technical Information Service
5301 Shawnee Rd., Alexandria, VA 22312
ph: (800) 553-NTIS (6847)
email: orders@ntis.gov <https://www.ntis.gov/about>
Online ordering: http://www.ntis.gov

PNNL- 33314

Noble Gas Management: SBMOF-1 vs. NUCON Carbon

September 2022

Praveen K. Thallapally
Alexander J. Robinson
Ali Zbib
Brian J. Riley
Saehwa Chong
Jian Liu
Mark K. Murphy
Parker Okabe[1]
Roman Sherrod[2]

Prepared for
the U.S. Department of Energy
under Contract DE-AC05-76RL01830

Pacific Northwest National Laboratory
Richland, Washington 99354

[1] Flibe Energy
[2] Flibe Energy

Summary

Pacific Northwest National Laboratory (PNNL), in collaboration with Flibe Energy, Inc., demonstrated the fabrication of metal organic frameworks (MOFs) into engineered beads to manage off-gases released from molten salt reactors. Among the many MOF options, SBMOF-1 was selected as an ideal sorbent to manage off-gases released from a molten salt reactor because its pore size is optimal. The SBMOF-1 was synthesized and fabricated into engineered particles using three different methods, with and without polymers. All the engineered particles were exposed to Co-60 radiation (1,000 kGy) to demonstrate their radiation stability. Single column breakthrough experiments were performed at different temperatures, activation conditions, flow rates, and off-gas compositions to optimize the Xe capacity at the breakthrough point and at saturation. The Xe loading in SBMOF-1 was compared with that of standard solid sorbent (NUCON carbon) under identical conditions. Based on the single column experiments, SBMOF-1 outperforms the NUCON carbon at all the temperatures and reduces the mass (to as little as 55%) of sorbent needed to achieve the same performance as carbon. The bed volume is also reduced, down to 48% of that of NUCON carbon, when the MOF is used. These results clearly demonstrate improvement in the amount of adsorbent needed and show a reduction in bed volume compared to traditional sorbent material.

This final report consists of two milestone discussions entitled, “Demonstrate Xe removal using engineered forms of MOF” (M3SB-19PN0201074) and “Optimization of single column breakthrough experiments” (M3SB-19PN0201075).

Acknowledgments

This effort was funded by a voucher from the U.S. Department of Energy (DOE) Office of Nuclear Energy's Gateway for Accelerated Innovation in Nuclear. We thank John Vienna and Mark Nutt of PNNL for helpful discussion and thoughts. We also appreciate helpful discussion and support from Flibe Energy personnel.

Acronyms and Abbreviations

BET	Brunauer-Emmett-Teller
DOE	U.S. Department of Energy
HKUST-1	copper-based MOF associated with Hong Kong University of Science and Technology
LFTR	liquid fluoride thorium reactor
MOF	metal organic framework
PAN	polyacrylonitrile
PMMA	poly methyl methacrylate
PNNL	Pacific Northwest National Laboratory
PXRD	powder x-ray diffraction
RGA	residual gas analyzer
RT	room temperature
SBMOF	Stonybrook metal organic framework
SDB	4,4' sulfonyldibenzoic acid
SEM	scanning electron microscopy
UiO	University of Oslo
XRD	x-ray diffraction

Contents

Figures

Tables

1.0 Introduction

The liquid fluoride thorium reactor (LFTR) introduces potentially unique challenges to the management of noble gas fission products. Because it uses a liquid fuel and actively removes the fission product xenon (Xe) by sparging the fuel with a noble gas, the LFTR can operate with highly dynamic loads. This is an asset for integration into a mixed energy generation portfolio that includes variable generation sources such as wind and solar power. This capability is impossible in solid fuel systems unless they incorporate a large amount of excess reactivity into the fuel to override the large neutron absorption cross section of Xe-135. However, active removal of noble gas fission products from the fuel salt also presents challenges to the facility design.

While noble gas fission products are bound inside the fuel in traditional nuclear power plants that employ metal-clad oxide fuel, liquid fueled reactors based on concepts such as the LFTR easily liberate the entirety of the noble gas fission product from the fuel form and must be designed to accommodate and contain that gas stream. Current technology for noble gas capture relies upon activated carbon to delay the flow of noble gases through an adsorber bed to decay short-lived isotopes. This approach requires very large adsorber beds (because these materials have lower adsorption capacities) to handle the noble gas stream from a utility class power reactor, which significantly increases the footprint of the nuclear island. This increase in footprint brings associated increases in cost, construction time, and operations and maintenance costs. Further, these adsorber beds are too large for some novel applications of LFTR technology, such as carbon-free power for commercial maritime shipping and bulk transport. Flibe Energy has received much investment interest from large maritime shipping organizations that have determined that nuclear energy is the only practical means to decarbonize their maritime operations. These operations require a highly dynamic, compact power source, for which the LFTR is well suited. However, the large gas management system compromises the applicability of the technology. To reduce the footprint of the noble gas system, we are exploring a new class of materials known as metal organic frameworks (MOFs) that might replace activated carbon materials.

Recently, crystalline microporous materials—including MOFs, porous organic cages, covalent organic frameworks, and zeolites—were demonstrated to separate xenon and krypton from each other and other off-gases near room temperature and over a relatively small footprint. (Riley et al. 2019; Elsaidi et al. 2020b; Salomon et al. 2015; Chui et al. 1999) In particular, MOFs are a very promising class of materials for selective removal of Xe and Kr because the pore size, shape, and specific surface area can be manipulated with the choice of organic building blocks and metal nodes. Materials with pore sizes just large enough to accommodate a single Xe atom or a single Kr atom would be ideal for separation.(Liu et al. 2014; Banerjee et al. 2016; Banerjee et al. 2015). Though MOFs have shown promise for noble gas separation, few or no efforts were found in the literature on the use of MOFs to manage noble gases released from molten salt reactors. Due to Environmental Protection Agency (EPA) and Nuclear Regulatory Commission (NRC) regulations, noble gases released from the LFTR fuel must be captured using delay beds to decay short- and long-lived fission gases, before the noble gases are separated using pressure- or temperature-swing adsorption using activated charcoal or cryogenic distillation (Riley et al. 2019). This approach requires very large adsorber beds (to compensate for the lower adsorption capacity) to handle the noble gas stream from a utility class power reactor, which significantly increases the footprint of the noble gas management system. This increase in footprint brings associated increases in cost, construction time, and operations and maintenance. Furthermore, in activated charcoal systems, the Xe is always

mixed with Kr-85 because carbon's selectivity is poor. Krypton-85 has a 10-year half-life, which renders the Xe unusable. An additional problem is that these adsorber beds are too large for some novel applications of LFTR technology. For example, it has been estimated that an 1100 MW boiling water reactor would require four to five charcoal beds with 6- to 9-ft-diameter, 50-ft-long delay beds (Nichols and Binford 1971) followed by series of charcoal beds to separate nonvolatile noble gases such as Xe and Ar, which have commercial value (Figure 1). This system is even less appealing given that the use of charcoal might result in bed fires resulting from the presence of oxygen and heat produced by radioactive decay. However, MOFs with higher specific surface areas, capacities, and selectivities would allow noble gas delay beds to be much smaller, more compact, safer, and more modular in design.

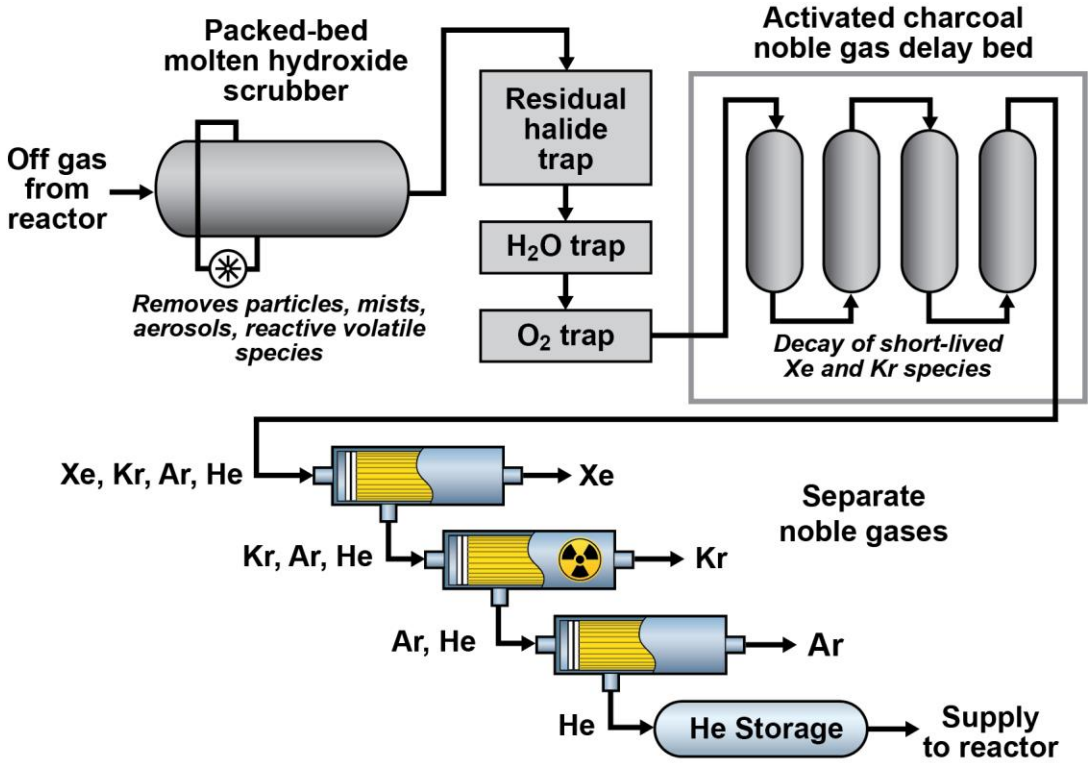

Figure 1. Schematic diagram of conventional off-gas management system for molten salt reactors. It consists of a series of traps to remove short lived volatile species, followed by noble gas decay tanks and pressure swing adsorption to separation noble gases. Modified from (Riley et al. 2019).

From the large body of MOF structures, we have selected CuBTC [a copper-based MOF, also known as HKUST-1 (Hong Kong University of Science and Technology)] as a potential sorbent because it is commercially available and has high specific surface area and pore volume (Elsaidi et al. 2020b; Salomon et al. 2015; Chui et al. 1999). Along with CuBTC MOF, PNNL evaluated UiO-67 (University of Oslo) MOF and three commercially available activated carbon materials for comparison (Alamo water carbon, Yakima carbon, and NUCON carbon). All three carbon materials appear to be of uniform size with particle sizes ranging from 200 µm to more than 1000 µm and were used without any further modification. The detailed synthesis and conversion of MOF powders into engineered forms using two different polymers including polyacrylonitrile (PAN) and poly methyl methacrylate (PMMA) were reported. Along with conversion, characterization of MOF engineered forms including powder x-ray diffraction (PXRD), Brunauer-Emmett-Teller (BET) surface area, scanning electron microscopy (SEM),

single component noble gas adsorption at different temperatures, and mechanical and radiation stability of the MOF powders and engineered forms were evaluated in greater detail (Elsaidi et al. 2020a; Riley et al. 2020). Over the course of testing, the UiO-67 and HKUST-1 MOFs performed poorly; however, the reasons for this poor performance were not clear and these materials require further evaluation. The possible reasons include pore blockage, inability to activate the engineered MOFs because an effective activation temperature would *exceed the melting point of the polymer* used, and possible equipment issues during the time we tested these materials.

Thus, a new MOF (Stony Brook Metal Organic Framework, SBMOF-1, also known as CaSDB) was added to the investigation, with and without binders. This MOF has previously been demonstrated for Xe/Kr separation at conditions relevant to nuclear reprocessing applications (similar to those needed for molten salt reactors) (Banerjee et al. 2016). The crystal structure of SBMOF-1 is shown in Figure 2 (Banerjee et al. 2012) In brief, the structure consists of Ca octahedra that connect with the V-shaped 4,4' sulfonyldibenzoic acid (SDB) linkers that form a square cross section with dimensions of 5.9 Å × 5.8 Å (Banerjee et al. 2012). A pore this size can fit a hard sphere up to 4.2 Å in diameter, which is slightly larger than xenon and optimally sized for its capture in preference to other noble gases (Banerjee et al. 2016). Therefore, experiments were performed to prepare the engineered form of SBMOF-1 with and without polymer (for mechanical stability) for tests using the gas composition found in the LFTR applications. The results allowed us to further optimize the performance of the SBMOF-1 engineered form at different temperatures and flow rates and compare its performance to that of NUCON carbon under identical conditions.

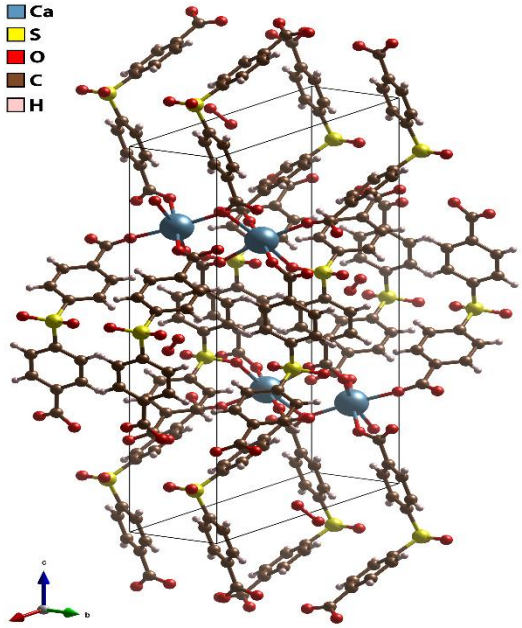

Figure 2. Crystal structure of SBMOF-1 viewed in the [211] direction from (Banerjee et al. 2012)

2.0 Synthesis and Characterization of CaSDB

The SBMOF-1 powder was synthesized from a previously developed procedure with some modification (Banerjee et al. 2016). Briefly, 4,4' sulfonyldibenzoic acid (SDB) ligand (98%, Alfa-Chemistry) and $CaCl_2 \cdot H_2O$ (>99%, Fischer Scientific) was measured in a molar ratio of 2:1 and were then dispersed in ethanol (Decon Labs, Inc.) using a 1:319 molar ratio between $CaCl_2 \cdot H_2O$ and ethanol. The reaction mixture was heated at 180°C for 72 hours while being stirred. After 72 hours, the reaction mixture was filtered and washed with ethanol before being dried in a vacuum oven at 60°C overnight. After the synthesis, the product was characterized using PXRD, BET, and Xe/Kr adsorption isotherm data.

XRD analysis was performed using a Bruker D8 Advance x-ray diffractometer (Bruker AXS Inc., Madison, WI) with a Cu source and a LynxEye position-sensitive detector. Powder samples were placed on zero-background quartz holders, and samples were scanned with a step of 0.02° and 1 s dwell time. Bruker AXS DIFFRAC^{plus} EVA (v4.1) was used for phase identification. The results of the XRD analysis are shown in Figure 3. As the figure clearly shows, the patterns of the simulated structure and the experimentally obtained pattern match each other quite closely, giving evidence that the synthesis successfully made the target SBMOF-1. BET analysis was done using a Micromeritics (Norcross, GA, USA) 3Flex surface characterization instrument while the powder was cooled to 77 K in a liquid nitrogen bath with nitrogen as the carrier gas. The BET surface area of this sample was measured at 248.66 m^2/g. This surface area was significantly higher than the reported literature value of ~140 m^2/g. Given the higher surface area of SBMOF-1, we anticipated a higher Xe/Kr adsorption. The isotherm data for Xe and Kr, shown in Figure 4 were obtained at 25°C for the high surface area sample along with a separate sample of SBMOF-1 that had a measured surface area of ~120 m^2/g. The data obtained show a quick uptake of Xe at low pressures, saturating around 1.45 mmol/g, which is nearly identical to previously reported data for SBMOF-1 despite the increase in surface area and is slightly higher than the lower surface area sample. The Kr adsorption was not as high at low pressure as the Xe uptake in that range and it saturated near 0.9 mmol/g, which is also close to the low surface area sample.

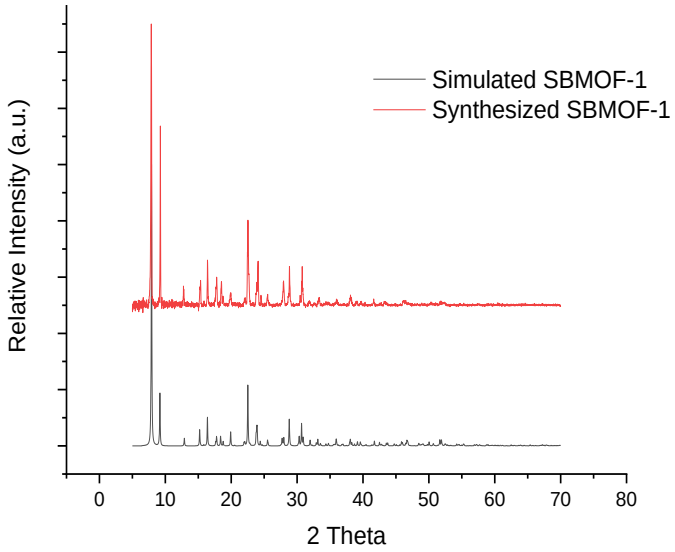

Figure 3. XRD pattern of obtained powder compared to simulated data

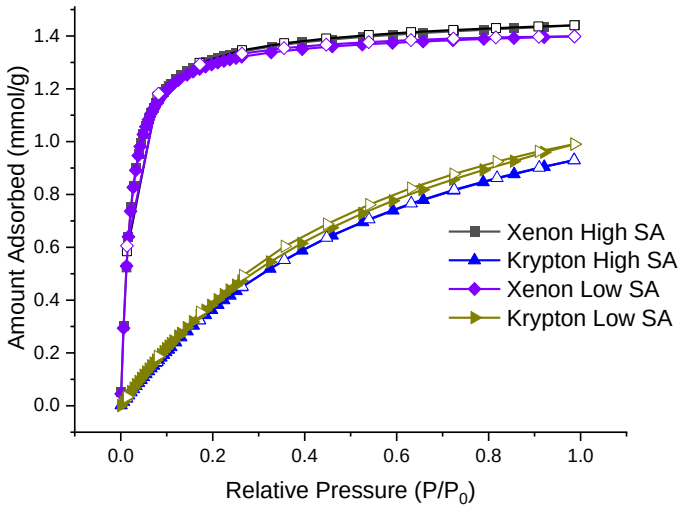

Figure 4. Xenon and krypton adsorption isotherms for high and low surface area samples of SBMOF-1

2.1 Fabrication of SBMOF-1 Pellets

The synthesized SBMOF-1 powder was turned into pellets with and without polymer using three different approaches. In the first method, the powder was pressed at 2000 psi to form tablets; this is shown in Figure 5 along with the other composite formation methods. These tablets were then passed through a sieve to get particle sizes in the range of 600 – 850 µm. The second method (Riley et al. 2020), involved dissolving 0.200 g of PAN fibers (X100 type, linear density 3.3 dtex, 60 mm long; Dralon GmbH, Dormagen, Germany) into 3.0 mL dimethyl sulfoxide (DMSO; ≥99.9%, Sigma Aldrich) at a ratio of 1 g of PAN per 15 mL DMSO and adding enough of the SBMOF-1 powder (1.800 g) to make it 9:1 by mass of MOF:PAN or 90 mass% MOF

solids loading in the final composite beads. This solution was then dripped from a 5-mL pipette tip into a deionized water (DIW) bath cooled to 5°C within a separate water bath, where the mixture pelletized into beads that were mostly spherical. The beads were washed in two subsequent DIW baths with a total residence time of ~5 min in each bath. After the second rinse, the composite beads were removed from the DIW bath, blotted dry on a paper towel, loaded into a glass vial, and dried in a vacuum desiccator for two weeks. The last method (Thallapally et al. 2019) used was wet granulation, where PMMA (25,000 MW, Polysciences, Inc.) was dissolved in dichloromethane (DCM; >99%, Sigma Aldrich) and the solution was added to an appropriate mass of SBMOF-1 to create a mixture that would be 9:1 by mass MOF:PMMA. This mixture was placed on a spinning rotor and the DCM was allowed to evaporate. While evaporating the DCM, the mixture was agitated by a spatula when a paste started to form. The paste was formed into granules, which were dried in an oven at ~100°C to remove any excess DCM. These granules were then also sieved to give the last set of composites to be tested.

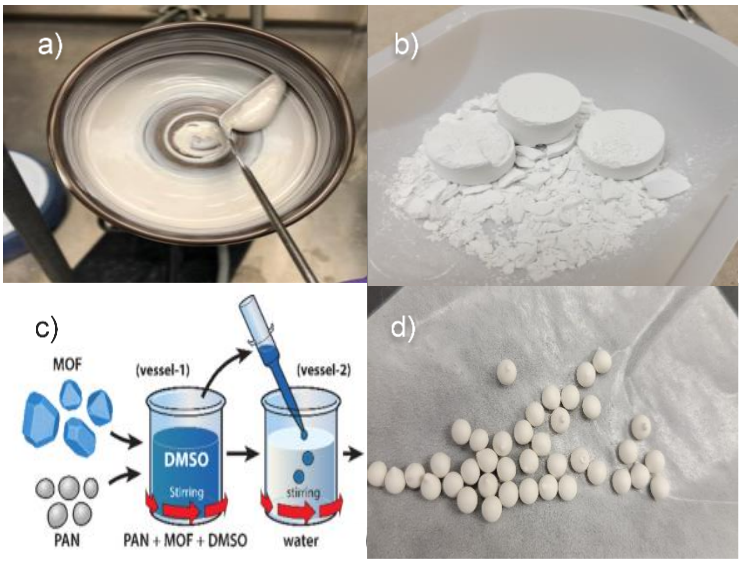

Figure 5. Fabrication of SBMOF-1 into engineered particles using different approaches: (a) Wet granulation method using PMMA polymer, (b) Applying 2k psi pressure to compact powder, (c) Schematic of PAN composite process, (d) 10% PAN SBMOF-1 composite material

2.2 Composite Characterization

The engineered forms underwent the same characterization techniques as the powder, with the addition of SEM imaging to examine how each method of composite fabrication affected its characteristics. To verify that the SBMOF-1 maintained its structure throughout the pelletization process, an XRD analysis was conducted. Figure 6 shows the results of the XRD and indicates that the underlying SBMOF-1 structure remained intact. Although the XRD produced the same peaks as the original powder, the relative intensities of those peaks varied, especially with the PAN composite material, which showed a significant reduction in intensity of the peak at ~9°

and an increase in intensity of the peak at ~13°. This change in intensity likely is caused by an orientation preference that forms during the process of making the PAN composite.

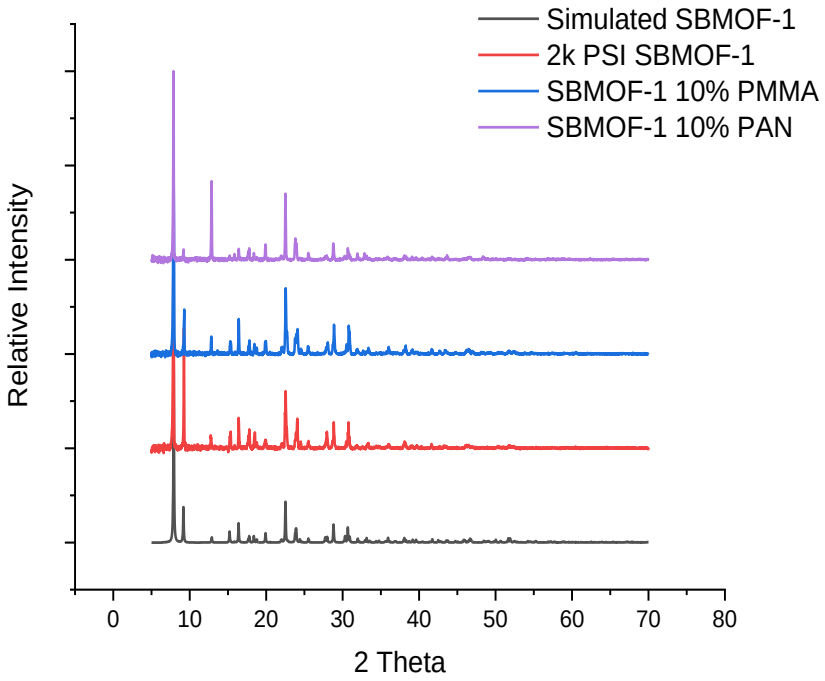

Figure 6. XRD data from the SBMOF-1 composites along with the simulated pattern from (Banerjee et al. 2012) for comparison

As summarized in Figure 7, the surface areas of the pressed pellets and the powder are relatively close to each other at 248.66 m^2/g and 245.43 m^2/g for the powder and pressed pellets, respectively. With the addition of 10% polymer to the MOF, the composite surface area dropped by nearly 30% for the PMMA composite, to 174.94 m^2/g, and by 38% for the PAN composite, to 155.44 m^2/g. This incommensurate drop in surface area is most likely caused by to the polymer blocking access to inner pore spaces in the composites, which would leave less surface area of the MOF exposed than just the 10% reduction from adding the 10% polymer.

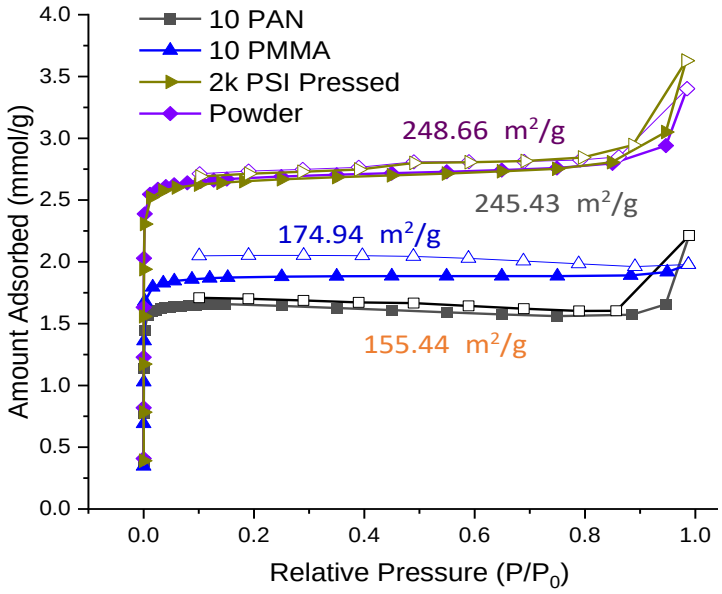

Figure 7. BET results of the different engineered forms of SBMOF-1 compared to the powder material

The reduction in surface area could compromise the ability to adsorb Xe and Kr, so Xe and Kr gas adsorption analysis was done on the samples to check whether it maintained its selectivity and capacity for those gases. The results of this measurement are shown in Figure 8. As expected, the pressed material did not show any deviation from the powder material when it came to its performance in adsorbing Xe. The composite materials, on the other hand, saw a ~15% reduction in capacity, slightly more than the expected 10% from adding polymer, but maintained a quick, steep uptake at low pressures, which is the region most of interest for its intended application. For Kr, the same trends hold, and the isotherms show no indication that the material would lose its ability to selectively separate Xe and Kr in the intended use in the low-pressure range. Though the polymers tend to block the pores, the composite particles remain porous.

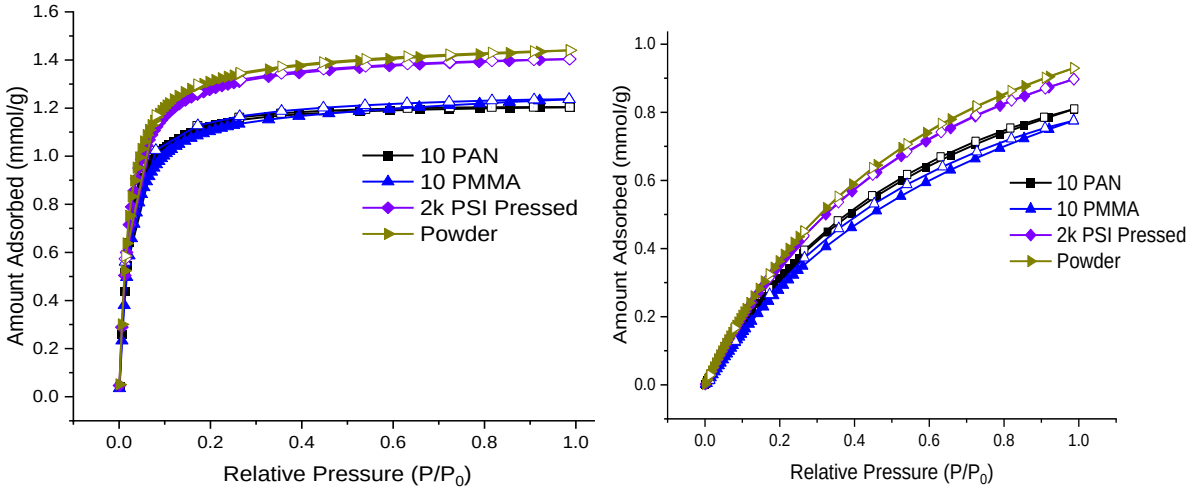

Figure 8. Adsorption isotherms of the different forms of SBMOF-1 for Xe (left) and Kr (right)

2.3 Radiation Stability

Our previous report dealt with the radiation stability of HKUST-1 and UiO-67 composites and a similar experiment was conducted on the SBMOF-1 composites (Elsaidi et al. 2020a; Riley et al. 2020). For radiation exposure, each set of pellets was exposed to 1000 kGy of radiation. This was done by placing the samples in a Co-60 gamma-ray field with the setup shown in Figure 9**.** The samples in this figure are secured in the beam port that would release the gamma-rays from a Co-60 source. The samples were equidistant from the source in this setup that allowed them to be exposed to gamma radiation at a rate of 70 kGy/hr. The samples were exposed to the radiation for the amount of time required to receive the intended dose and then they were further characterized by XRD and SEM for comparison with their unirradiated counterparts. The XRD results after irradiation are shown in Figure 10. The patterns prior to irradiation match well with the post-irradiation patterns and no significant deviations were seen from them that would indicate any deformations in the structures. This indicates that the SBMOF-1 crystal structure is stable under irradiation up to at least 1000 kGy. In addition to the XRD, SEM analyses were performed to obtain surface topography of the particles before and after irradiation. The SEM results show that the crystal structure was maintained. The SEM and energy-dispersive x-ray spectroscopy analyses were performed with a JSM-7001F field-emission gun microscope (JEOL USA, Inc.; Peabody, MA). Samples were not coated and were analyzed in low-vacuum mode (30 Pa) to prevent charging artifacts. The images from the SEM are shown in Figure 11.

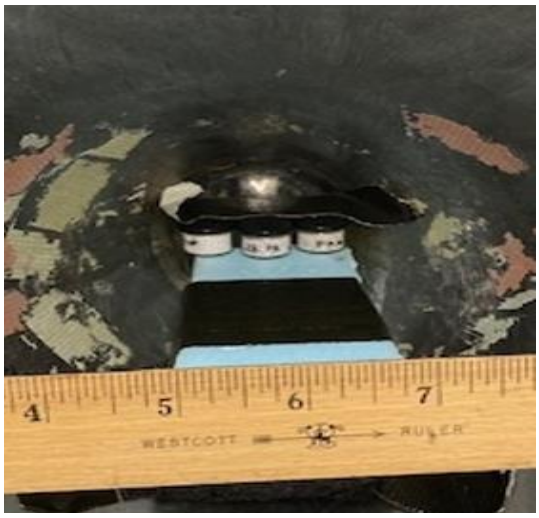

Figure 9. SBMOF-1 composites secured in Co-60 gamma-ray beam port.

From the SEM images, no noticeable difference was observed between the unirradiated and irradiated samples. This lack of change coupled with absence of changes in the XRD pattern indicate that the composites and the MOF can withstand exposure to radiation and remain stable.

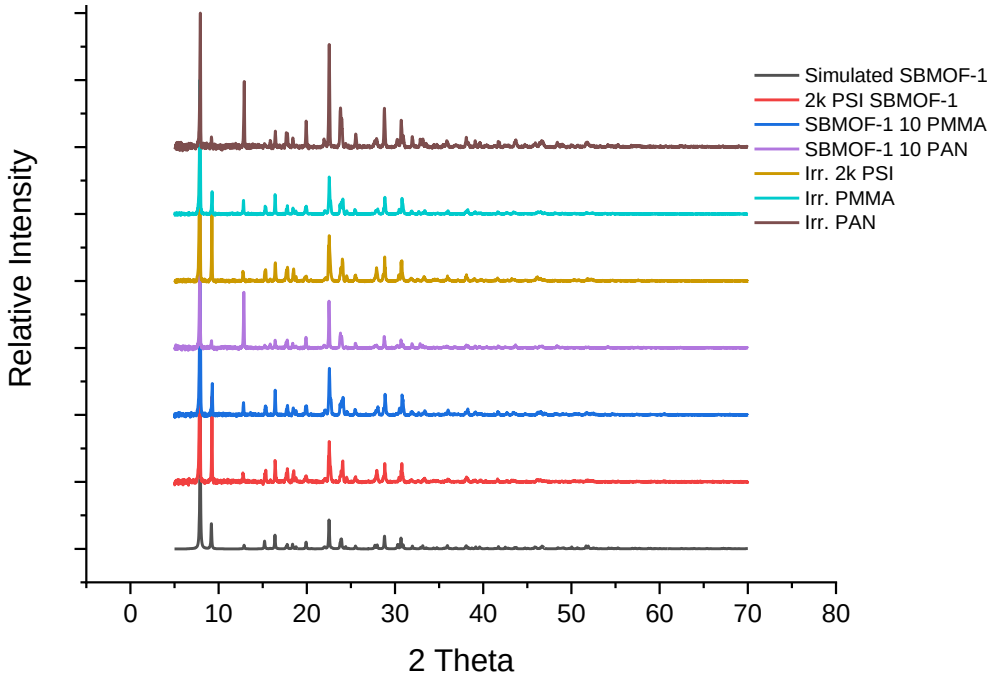

Figure 10. XRD results from irradiated and unirradiated samples

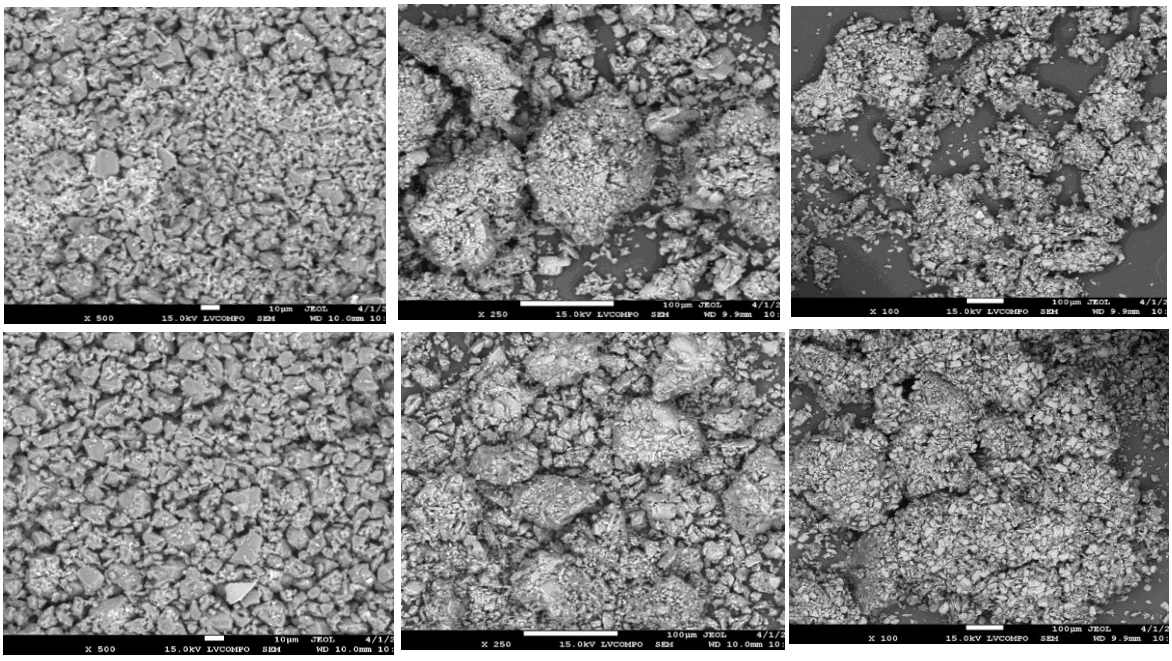

Figure 11. SEM images of SBMOF-1 samples before (top row) and after irradiation (bottom row): 2k psi pressed SBMOF-1 (left), 10% PMMA SBMOF-1 composite (middle), and 10% PAN SBMOF-1 composite (right).

2.4 Breakthrough Measurements

Previously, we conducted experiments exposing our target MOFs to single component gases to record adsorption isotherms of Xe and Kr at 1 bar pressure and room temperature. In breakthrough experiments, the dynamic adsorption of the MOFs can be measured by running multicomponent gases through an adsorption column and measuring the gas composition after it flows through the column. The schematic diagram for the breakthrough experiment is shown in Figure 12. In the experiment, two lines, containing an inert gas (He) and an analysis gas, were deployed and connected to a three-way valve. This valve allowed for quick switching between the inert and analysis gases. Each gas line also featured a pressure regulator and a mass flow controller. The pressure regulator was used to introduce the gases at the same pressure and the mass flow controller maintained the flow of gas into the three-way valve at a constant rate. The mass flow controllers were calibrated using a bubble meter and all flow rates used were interpolated from a calibration curve. As shown in Figure 12, a water bath extension was available to introduce humidity into the gas stream. We did not study in detail the effect of humidity on the Xe/Kr removal, but this capability is present in case humidity variation needs to be evaluated in future.

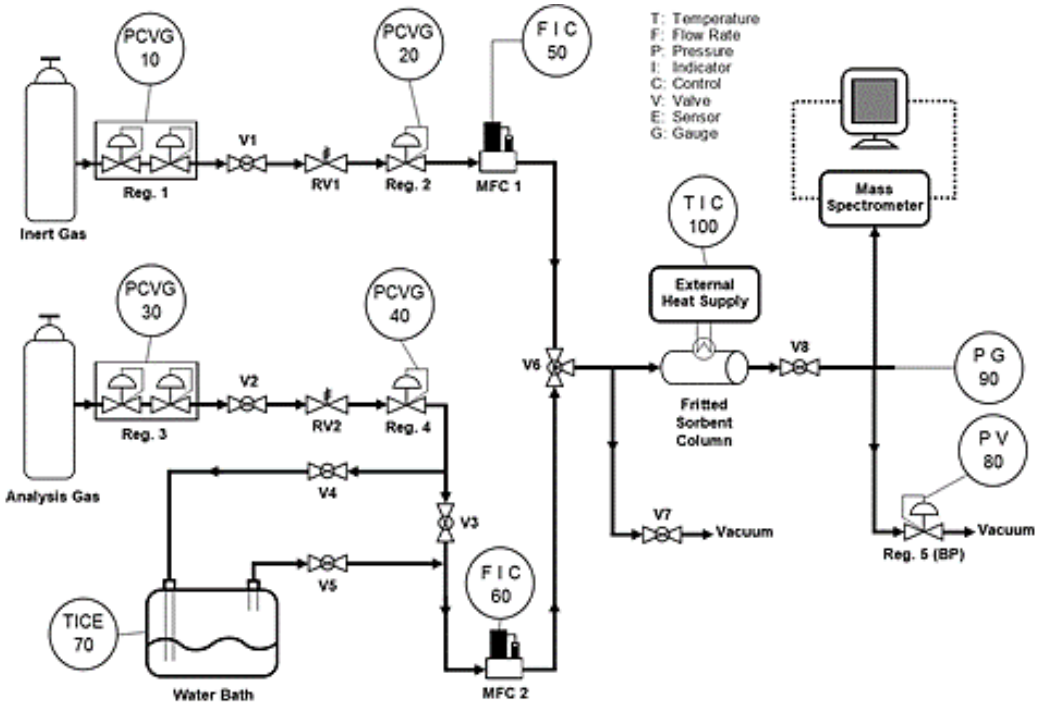

Figure 12. Process flow diagram of breakthrough apparatus

After the three-way valve, a vacuum line was added to the column to activate the materials and remove any residual gas from the column and between runs. The column itself, shown in Figure 13, is enclosed in an insulated container and surrounded with fiberglass to help maintain experimental temperature, especially during runs at −40°C. Around the column is a heating block that is used to set the temperature of the column during an experiment. Four holes are drilled into the heating block, two of which are threaded. As shown in Figure 13, one of the threaded holes holds a screw that is connected to a grounding wire to make sure the system shuts off in case the column becomes energized. The two non-threaded holes are used to fit thermocouples, one of which is used in conjunction with the heating block and the other to

connect to an overtemperature controller. The column is 3" long and 1/4" in diameter. Both ends of the column are fitted with 0.5-micron-mesh frit to keep the material in the column while gas is flowing. Beyond the column are a pressure gauge, a pressure transducer, and a needle valve connected in a three-way split. The pressure gauge gives feedback to the transducer such that the column can be maintained at a specified pressure. For these experiments, the pressure is maintained at 18.85 psi or ~1.3 bar. The needle valve leads to a residual gas analyzer (RGA), which measures the gas composition exiting the column. The pressure in the RGA is maintained at ~2×10^{-7} torr when an experiment is not running. During the experiment, the pressure reading from the RGA is kept below 5×10^{-5} torr to not overburden the turbo pump and scroll pump combination needed for the RGA to properly function.

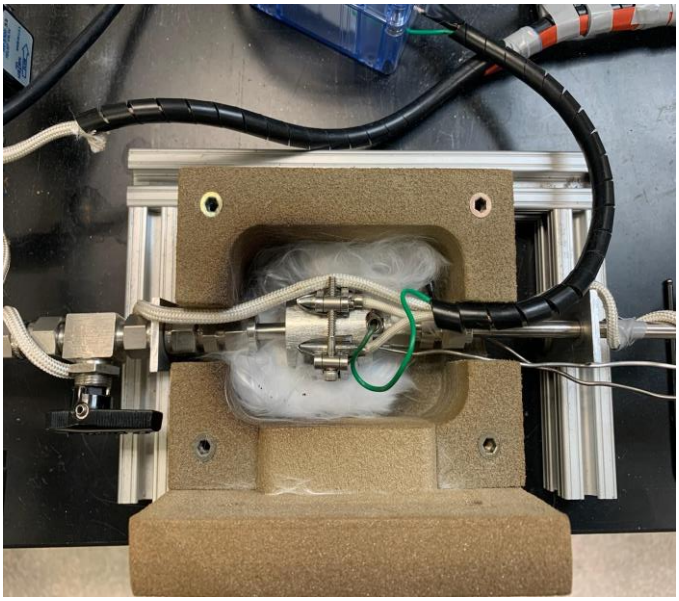

Figure 13. Column setup during an experiment

To run experiments at subzero temperatures, a special setup was used and is shown in Figure 14. The apparatus consists of a micro-dosing liquid nitrogen pump and an off-gas delivery system. The micro-dosing system works by sending electric current pulses to a resistive element attached to the system that heat the resistive element; the heat is transferred to the liquid nitrogen in the container. This heat will boil some of the liquid nitrogen, which then flows into the off-gas tubing. This off-gas tubing is positioned next to the column to provide cold nitrogen gas to cool it.

Figure 14. Micro-dosing liquid nitrogen system

2.5 Breakthrough Procedure

During a typical run, the column is filled with the test material, which has a diameter of 600–850 mm; (the glass beads used in a blank run are ~1 mm in diameter). The mass of material added is recorded and it is placed within the breakthrough setup. The sample is activated in the apparatus by exposing it to vacuum while heating it to beyond 180°C, but below the column temperature limit of 200°C. After activation, the column is cooled to the desired experimental temperature, and either cool compressed air or liquid nitrogen off-gas blows on the column to help maintain the experimental temperature.

Once the desired temperature is reached, the RGA is turned on and exposed to the empty capillary tubes that follow the needle valve connected to the column. These capillary tubes are cleared of any gas before the column under vacuum is exposed to the RGA. If the pressure reading on the RGA is relatively high while it is reading the gas composition of the vacuumed column, the experiment will not begin, and more time will be given to vacuum out the column before gas flow begins. After the RGA reads the composition of the gas from the vacuumed column for 5 minutes, helium gas flow is started through the column. The flow rates of helium and the analysis gas during an experiment are set to either 10, 15, or 20 mL/min and will be the same for both gases during a run. Helium is the first gas through the column during an experiment because it will help purge the column of any residual gases and provide a background signal that can be monitored to help determine when gas flow changes to the analysis gas. The He is usually allowed to flow through the column for ~15 minutes, during which the pressure transducer is adjusted to maintain pressure at 18.85 psi. Once 15 minutes have passed, the three-way valve is switched to the analysis gas to begin running the breakthrough experiment. The analysis gas runs through the column until it is determined that the column has reached the saturation pressure for all analysis gases or until a breakthrough point for Xe is observed. After it is determined that all gases have broken through the column and the test material, the three-way valve is turned back to He. The He is allowed to flow through the column and into the RGA for ~10 minutes to note any changes that occur in the He

signal from those at the start of the run. After this, the needle valve leading to the RGA is closed, all gas flow through the column stops, and the column is once again placed under vacuum to activate the sample for the next run.

2.6 Demonstrate and Optimize Xenon Removal using 2k Pressed SBMOF-1

Figure 15 shows the breakthrough results for the SBMOF-1 pressed particles at room temperature with a flow rate of 10 mL/min using two different gas compositions: (a) simulated LFTR off-gas (1000 ppm Xe, 100 ppm Kr, Ar balance) and (b) air-balanced off-gas (1300 ppm Xe, 130 ppm Kr, air balance) to help evaluate the effect the competing gases (CO_2, O_2, and N_2 in the air) have on the adsorption of xenon. The *x* axis represents the time it took for each gas to exit the column and the *y* axis (C/C_0) shows the concentration of outlet gas as a fraction of the concentration of the inlet gas. In the figure, it can be clearly seen that Xe breaks through the column much later than the other gases present in the off-gas.

The Xe breakthrough and saturation capacities were calculated using the breakthrough plot and the ideal gas law. The breakthrough capacity is calculated from the point where Xe first appears to have a detectable signal in the RGA. In Figure 15, the breakthrough point for Xe was around 3900 s. The volume of gas can be calculated by multiplying the flow rate (10 mL/min) by the time it took for breakthrough (3900 sec). Using the assumptions of the ideal gas law, the moles of Xe that pass through the column will be the total number of moles multiplied by the volumetric ratio of Xe in the gas mixture. The Xe breakthrough capacity can be calculated by dividing the adsorbed Xe by the mass of the activated sample. Similarly, the saturation Xe capacity can be calculated by dividing the saturation Xe capacity (counting from the beginning to the point where the outlet Xe concentration reached the inlet concentration) by the mass of the activated sample. The saturation capacity represents the total amount of gas that the sorbent held throughout the run. The breakthrough capacity for 2k-psi-pressed SBMOF-1 was calculated as 42 mmol/kg and the saturation capacity as 75 mmol/kg.

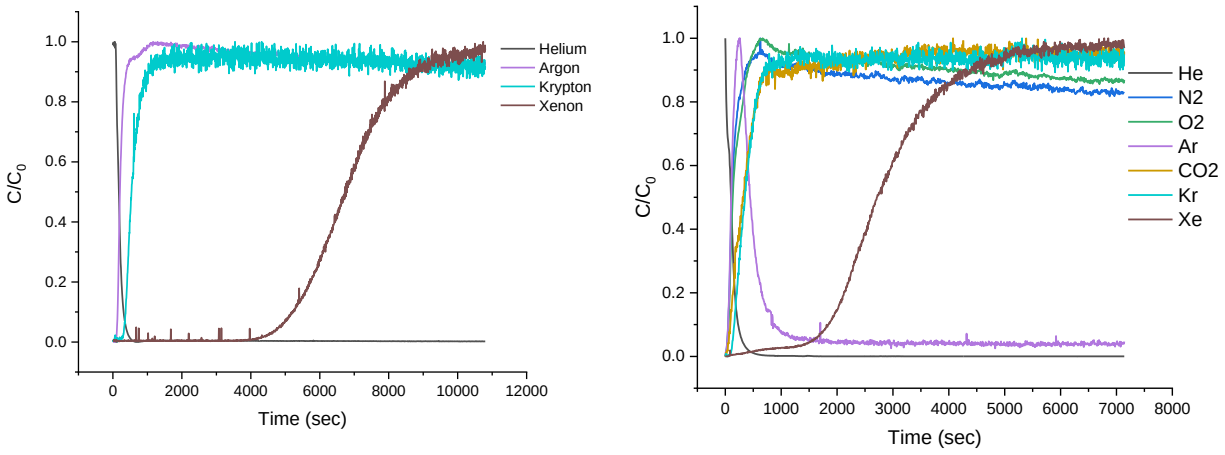

Figure 15. Breakthrough curves at 25°C with flow rate of 10 mL/min for simulated LFTR off-gas (left) and air-balanced off-gas (right)

Further, breakthrough capacities were optimized by performing the same experiments at different temperatures and flow rates. The cycle stability was also investigated using 2k-pressed particles by activating the sample at 100°C under vacuum between the runs. Table 1 and

Table 2 provide the Xe capacities at breakthrough and saturation under different experimental conditions.

Table 1. Single column breakthrough experiments using two different off-gas compositions using SBMOF-1 engineered particles: (a) 1000 ppm Xe, 100 ppm Kr balanced with Ar and (b) 1300 ppm Xe, 130 ppm Kr balanced with air at different temperatures, keeping other parameters constant.

Off-gas	Xe concentration (ppmv)	Activation temperature (°C)	Experiment temperature (°C)	Flow rate (mL/min)	Capacity at breakthrough (mmol/kg)	Capacity at saturation (mmol/kg)
Simulated LFTR off-gas	1000	125	25	15	39	75
	1000	125	0	15	166	NA
Air-balanced off-gas	1300	125	25	10	38	82
	1300	125	0	10	211	NA

Table 2. Xe loading at breakthrough and saturation capacities at different temperatures

Off-gas	Xe concentration (ppmv)	Activation temp (ºC)	Experiment temperature (ºC)	Flow rate (mL/min)	Capacity at breakthrough (mmol/kg)	Capacity at saturation (mmol/kg)
Air-balanced off-gas	1300	125	0	10	211	N/A
	1300	125	−40	20	804	N/A

For the pressed particles, three main variables were changed: the Xe concentration, the experimental temperature, and the flow rate. From Table 1, the higher Xe concentrations in the off-gas yielded slightly higher capacities than the lower Xe concentrations under the same column packing. This is expected because this off-gas has a higher xenon concentration than the simulated LFTR off-gas. The higher capacity is more pronounced in low temperature experiments than at room temperature (RT). The competing gases added to the simulated off-gas (CO_2, O_2, and N_2) did not show any significant adsorption or competition with Xe for the SBMOF-1, which shows that the MOF is selective with those gases present as well.

The second variable tested with the pressed material was the experimental temperature. The experiments indicate temperature is the single greatest factor affecting the Xe capacity. From Table 1, the Xe breakthrough capacity of the simulated LFTR off-gas increased from 39 mmol/kg to 166 mmol/kg when the experimental temperature was decreased from 25°C to 0°C. A similar increase is shown in Table 2 when temperature was decreased from 0°C to −40°C, where breakthrough capacity increased from 211 mmol/kg to 804 mmol/kg using slightly higher concentrations of Xe and there was no effect on Xe loading in the presence of N_2, O_2, Ar, etc.

The third and final variable tested with the pressed material was the flow rate of the gas through the column. Flow rates tested were 10 mL/min and 15 mL/min; 20 mL/min was exclusively used to obtain −40°C data because obtaining a breakthrough point at that temperature required a great deal of time. The amount of gas needed for the −40°C runs also limited this test to only

using the 1300 ppm Xe gas canister because the supply from the 1000 ppm Xe cylinder was limited. From the data in Table 1 and appendix Table A4, there were no significant changes in breakthrough capacity or saturation capacity when different flow rates were used with these samples.

Cyclic stability of the pellets under varying conditions was also tested. Table A4 shows the results of repeated cycling of the material through the capture and degas process. This was done by first exposing the column to the test gas and then activating the adsorbent overnight under vacuum to recycle the material for the next test. The data from these points remain relatively constant and consistent for testing under the same conditions, showing no extreme changes in saturation or breakthrough capacity between runs under similar conditions. These results show that the pellets can be used multiple times to capture xenon.

2.7 Comparison of SBMOF-1 Pressed Particles vs. NUCON Carbon

To compare the performance of SBMOF-1 with NUCON carbon (as a standard), similar breakthrough experiments were performed using NUCON carbon. NUCON carbon was sieved to obtain particles 600 μ to 850 μ in diameter. Single column breakthrough experiments were performed using 0.6117 g of carbon as adsorbent at different temperatures using simulated LFTR off-gas composition at 25°C and 0°C, and at −40°C using off-gas composition containing 1300 ppmv Xe and 130 ppmv Kr balanced with air. The Xe breakthrough curves from each experiment are shown in Figure 16 compared to the Xe breakthrough curves for SBMOF-1 under identical conditions. The saturation capacity, breakthrough capacity, and experimental conditions are summarized in Table 3. From Figure 16, SBMOF-1 clearly features a much greater capacity for Xe than that of NUCON carbon at all temperatures tested.

This superior performance of SBMOF-1 over NUCON carbon can be translated into differences in the total sorbent mass and bed volume required for the separation, which are shown in Figure 17. To obtain the same performance as carbon in terms of Xe removal efficiency, at different temperatures, the masses of SBMOF-1 required would be 82%, 55%, and 74% of those for NUCON carbon at 25°C, 0°C, and −40°C, respectively (Figure 17). For example, at 0°C, replacing NUCON carbon with SBMOF-1 would require only 55 grams to every 100 grams of NUCON carbon. In addition to the reduction of mass, the packing density of SBMOF-1 (0.633 g/cc) is greater than that of NUCON carbon (0.55 g/cc) (Welty et al. 2018). This difference in packing density would also reduce the volume of the column needed to do the separation. At 0°C, the volume of the column would be reduced to 48% of that needed if NUCON carbon were the sorbent. This is the optimum condition for replacement of NUCON carbon with SBMOF-1, though operating at −40°C would reduce the overall amount of SBMOF-1 the most.

The data in Figure 17 show that SBMOF-1 can be a suitable replacement for NUCON carbon; however, the mechanical stability experiments indicate that the pressed SBMOF-1 powder might not be strong enough for the end use application. This lack of mechanical strength led to the initial desire to test polymer composites using PAN and PMMA. The PAN and PMMA composites were shown to have better mechanical stability than their pressed counterpart.

Table 3. Xe breakthrough and saturation capacities for NUCON carbon using LFTR off-gas composition at different temperatures.

Xe concentration (ppmv)	Experiment temperature (°C)	Flow rate (mL/min)	Breakthrough capacity (mmol/kg)	Saturation capacity (mmol/kg)
1000	25	15	32.1	58
1000	0	15	91.2	156
1300	−40	20	596.9	824

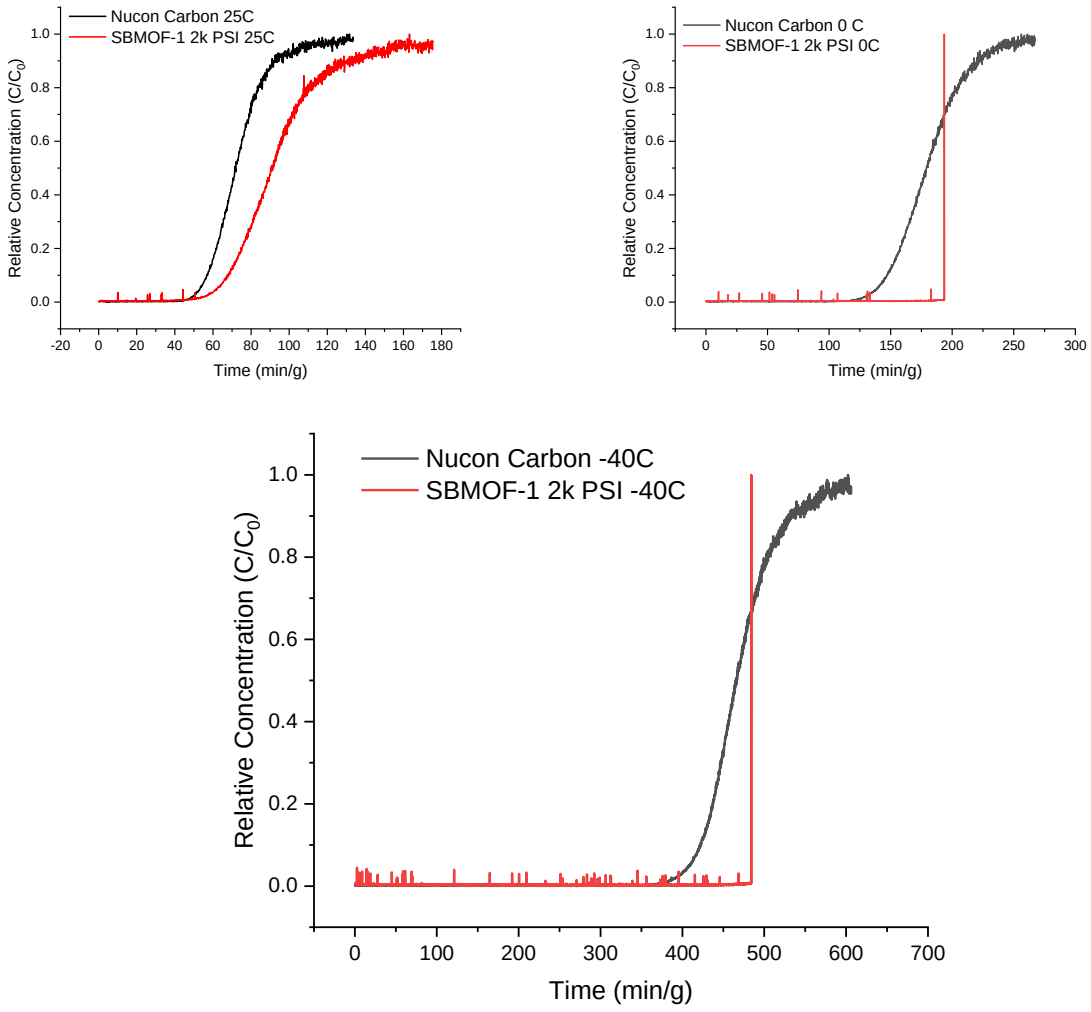

Figure 16. Single column breakthrough curves for SBMOF-1 and NUCON carbon at 25°C (top left), 0°C (top right), and −40°C (bottom). Plots for other gases were removed for clarity. The sharp breakthrough (red line) is the result of long breakthrough times when MOF is used, and the experiment was halted.

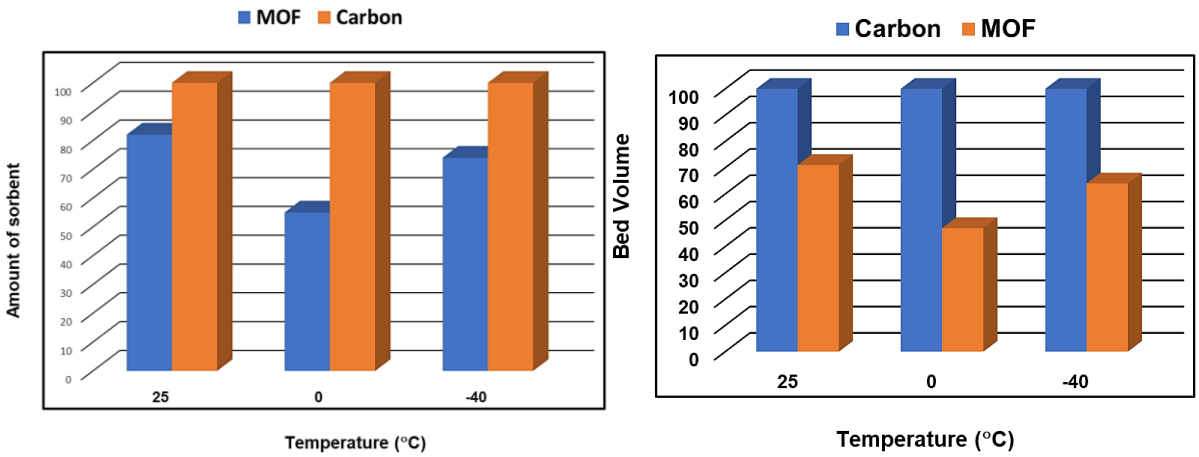

Figure 17. Relative masses and bed volumes needed for SBMOF-1 when normalized to carbon

2.8 Demonstrate and Optimize Noble Gas Performance Using SBMOF-1 PAN Composites

As discussed above, two different SBMOF-1 composites using well-known binders (PMMA and PAN) were fabricated and characterized. As shown in Figure 18, both composite materials have very sharp Xe loading at RT, though they have 15% lower Xe capacity than the pressed SBMOF-1 particles. To demonstrate Xe removal from the simulated LFTR off-gas, single column breakthrough experiments were performed using both composites.

First, 0.3613 g of SBMOF-1 PAN composites were loaded into the column, activated at 100°C under vacuum overnight, and cooled back to RT. Figure 18 shows an equilibrium capacity of 20 mmol/kg at RT, significantly lower than that of SBMOF-1 pressed particles under identical conditions. Next, the Xe equilibrium capacity was optimized by activating the SBMOF-1 PAN composites at higher temperatures. As shown in Figure 18, the Xe equilibrium capacity increased as a function of temperature. At 180°C, the Xe equilibrium capacity reached 45 mmol/kg at RT. Next, we kept all the parameters including flow rate, gas composition, and activation temperature (150°C) constant and varied the experimental temperature. Figure 19 shows the Xe capacity at equilibrium and breakthrough point. The Xe capacity increased as the temperature decreased, which was expected; however, when compared to SBMOF-1 pressed particles and NUCON carbon, the Xe loading in the PAN composite is significantly lower. In addition to the lower capacity, the breakthrough curve from the PAN composite is qualitatively different from those obtained from NUCON carbon and the pressed SBMOF-1 pellets.

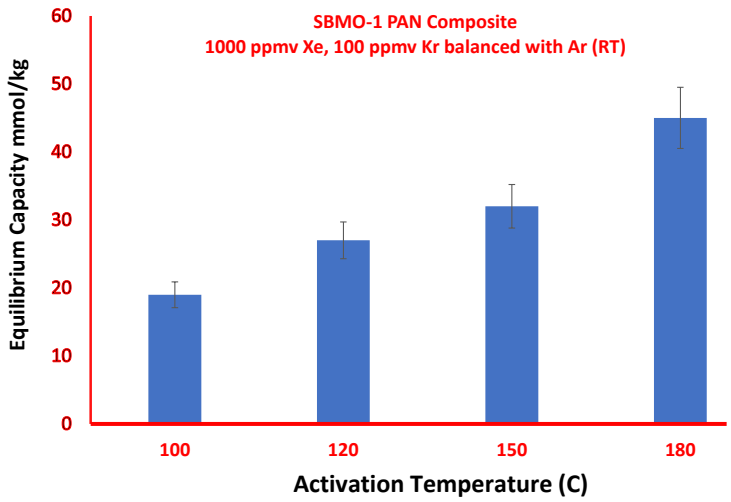

Figure 18. Equilibrium capacity as a function of activation temperature for SBMOF-1 PAN composites

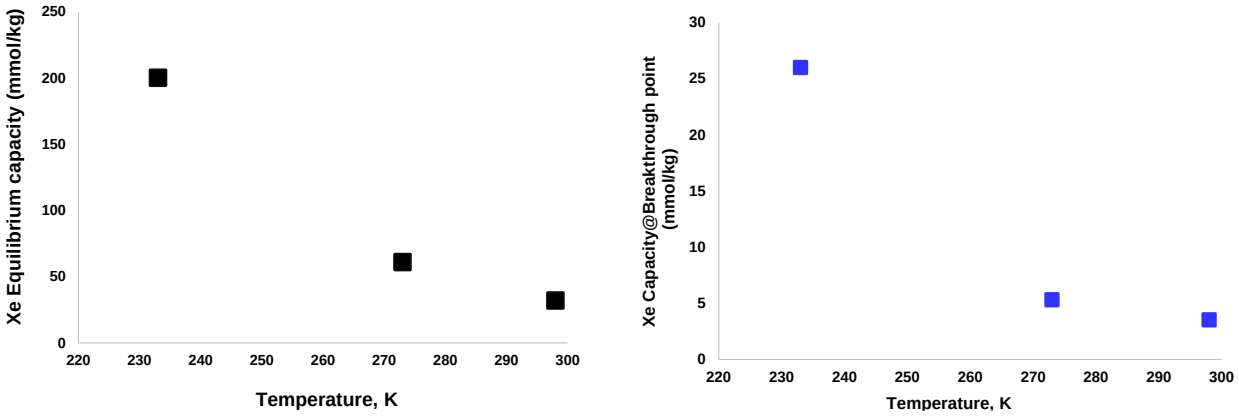

Figure 19. Equilibrium (left) and breakthrough (right) capacities of SBMOF-1 PAN composites at different temperatures.

Figure 20 shows the breakthrough curves of the PAN composite, pressed pellets, and NUCON carbon. From this figure, it can be seen that breakthrough curves for NUCON carbon and pressed SBMOF-1 have long deadtimes and quick saturation after the initial breakthrough. The composite material, however, has a short deadtime and breaks through almost immediately, but takes a long time to reach saturation. This change in kinetics is thought to be caused by the polymer introduced to SBMOF-1 powder. The polymer may be blocking access to adsorption sites in SBMOF-1, allowing Xe to pass through the column quickly. These binding sites, however, are still functional, but take longer to reach equilibrium. The capacity at the breakthrough point for SBMOF-1 PAN composite is 5.12 mmol/kg at RT and can be compared to 32.1 mmol/kg for NUCON carbon and 39.1 mmol/kg for 2k psi pressed particles. The equilibrium capacity was 45 mmol/kg at RT for SBMOF-1 PAN composites, which can be compared to 58 and 75 mmol/kg for NUCON carbon and SBMOF-1 pressed particles, respectively. The loss of capacity can be attributed to inclusion of polymer, but the amount of SBMOF-1 required to match the performance of NUCON carbon at RT was calculated to be 82%. The 10% loss from adding polymer and 15% reduction of Xe capacity should have still allowed the composite to outperform NUCON carbon, but, as mentioned, the polymer's

inclusion changes the adsorption kinetics, leading to the composites being outperformed by NUCON carbon at every tested temperature. The rest of the results for the PAN composite are summarized in Table 4–Table 6. Additionally, there was a significant difference in performance observed when using different flow rates at RT. This was repeatable and suggests that flow rate could play a part in optimizing performance when it comes to fully implementing these columns in an off-gas system with PAN composites. Despite this observation, this phenomenon did not persist when lower temperatures were tested. Further testing using a large amount of material is needed to optimize these results in a more controlled environment.

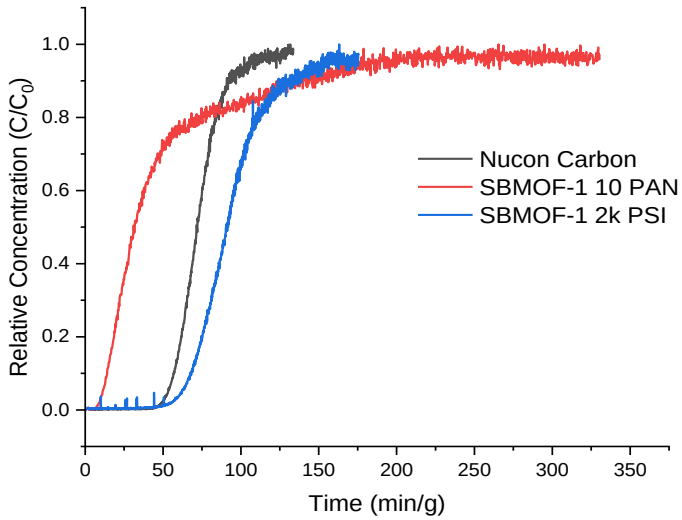

Figure 20. Xenon breakthrough curves for each sorbent tested at 25°C with a flow rate of 15 mL/min

Table 4. Xe capacity at breakthrough and saturation as a function of activation temperature.

Xe concentration (ppmv)	Activation temperature (°C)	Experiment temperature (°C)	Flow rate (mL/min)	Capacity at breakthrough point (mmol/kg)	Capacity at saturation (mmol/kg)
1000	100	25	15	1.56	21
1000	150	25	15	3.52	32
1000	180	25	15	5.12	45

Table 5. Xe capacity at breakthrough and saturation point as a function of experimental temperature using SBMOF-1 10%PAN (Keeping all other parameters constant)

Xe concentration (ppmv)	Activation temperature (°C)	Experiment temperature (°C)	Flow rate (mL/min)	Xe capacity at breakthrough point (mmol/kg)	Xe capacity at saturation (mmol/kg)
1000	150	RT	15	3.52	32
1000	150	0	15	5.31	61
1000	150	−40	15	25.99	~200

Table 6. Breakthrough Results SBMOF-1 10% PAN

Xe concentration (ppmv)	Experiment temperature (°C)	Flow rate (mL/min)	Breakthrough capacity (mmol/kg)	Saturation capacity (mmol/kg)
1000	25	10	3.53	31
1000	25	15	5.12	45
1000	25	20	3.52	32
1000	0	10	5.15	62
1000	0	15	5.31	61
1000	−40	10	29.91	200

2.9 Demonstrate and Optimize Noble Gas Performance Using SBMOF-1 PMMA Composites

As with SBMOF-1 pressed particles and SBMOF-1 PAN composites, single column breakthrough experiments were performed using the newly developed SBMOF-1 PMMA composite to address some of the limitations that arose in SBMOF-1 PAN testing. For example, SBMOF-1 PAN tends to have better mechanical stability, but the Xe loadings at breakthrough point and equilibrium were significantly lower than those of SBMOF-1 pressed particles. This was partly attributed to the temperature required to activate the SBMOF-1 PAN composites: a high boiling point solvent such as DMSO must be used to prepare them. Hence, these composites must be activated beyond 180°C. After repeated activation of SBMOF-1 PAN composites at 180°C, the PAN composite was discolored, as shown in Figure 21. This is partly caused by the uneven heating of the column. After careful characterization of the discolored particles, the XRD showed that the MOF retained its structural topology and morphology, but decomposed products could block the pores of the SBMOF-1 and reduce its capacity.

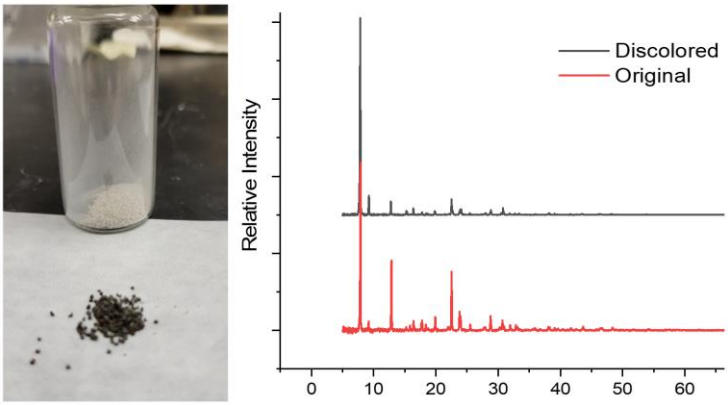

Figure 21. Discolored PAN composite and its XRD pattern change

This led to the investigation of the other polymeric binder (PMMA). The detailed fabrication of SBMOF-1 PMMA composites and their characterization were discussed above. Single column breakthrough experiments using SBMOF-1 PMMA composites were performed under conditions identical to those for the other composites. The breakthrough results for the PMMA composite, shown in Figure 22 and Table 7, were among the worst tested in this effort, showing significantly lower adsorption even than the PAN composite. In addition to poor results, the performance of

the composite degraded over the course of testing, as demonstrated by a significant drop in performance for the −40°C run from 110 mmol/kg to 39 mmol/kg. This was followed up with reruns of 25°C data, which also saw significantly lower capacities. As a result of this sudden decrease, XRD analysis was done on the pellets after removed from the column; the results are shown in Figure 22. The XRD results (Figure 23) show that the pattern has shifted to the higher angles and the peaks have broadened. The shift to higher angles could indicate that the crystal lattice has shrunk, and the broadening of the peaks means that it has lost some of its crystallinity. The cause of both is thought to be the melting of the PMMA polymer. PMMA has a relatively low melting point, at 160°C. The SBMOF-1 was activated at 135°C, but that added heat could have softened the PMMA and allowed it to flow and constrict the underlying SBMOF-1 structure. This constriction reduced the MOF's capacity. The overall results from the testing suggest that PMMA is not a suitable binder for this material.

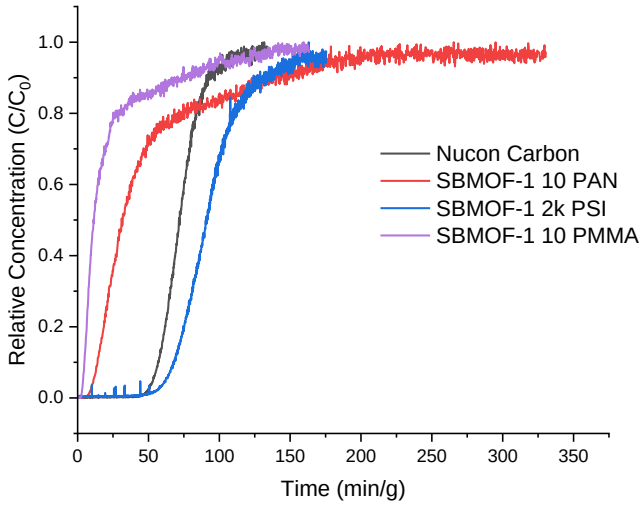

Figure 22. Xenon breakthrough curves for SBMOF-1 composites and NUCON Carbon

Table 7. Xe breakthrough and saturation capacity for SBMOF-1 10% PMMA composite at different temperatures using simulated LFTR and reprocessing off-gas mixture

Xe concentration (ppmv)	Experiment temperature (°C)	Flow rate (mL/min)	Breakthrough capacity (mmol/kg)	Saturation capacity (mmol/kg)
1300	25	15	1.5	31
1300	25	15	1.93	26
1300	25	10	1.98	29
1000	25	10	1.98	29
1000	25	15	1.93	26
1300	−40	15	5.65	69
1300	−40	15	4.25	110
1300	−40	15	1.98	39
1000	25	15	1.31	17
1000	25	10	1.38	16

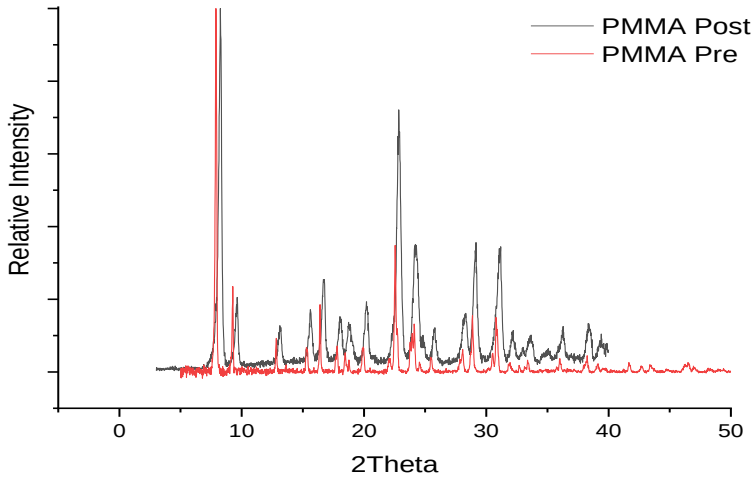

Figure 23. XRD patterns of SBMOF-1 PMMA composite before (Pre) and after (Post) breakthrough experiments

2.10 Modeling the adsorbed beta dose in MOF

For a 600 MW_{th} reactor fissioning U233, cumulative fission product yield for all xenon isotopes with half-lives greater than one minute were calculated as 1.94e-6 g/s. An upper bound on the average absorbed dose in the MOF was calculated assuming all the xenon survives long enough to be captured. The relevant unstable isotopes of Xe undergo beta decay. Since the beta particles are expected to dominate the material damage to the MOF, the gamma dose was determined to be insignificant and ignored for this calculation. The beta particle energy for a given decay was treated as equal to the average beta particle energy for that decay. A standard

50 L tank can hold 31650 g of MOF, and can capture 8.23 g of Xe before breakthrough, which will take 49.05 days. During this time while the Xe accumulates and decays in the MOF, 1.27e25 keV will be released in beta particle kinetic energy. Given that the gaseous Xe will be suspended within the MOF, all this energy is expected to be absorbed within the MOF. This results in an absorbed dose of 64.2 Gy.

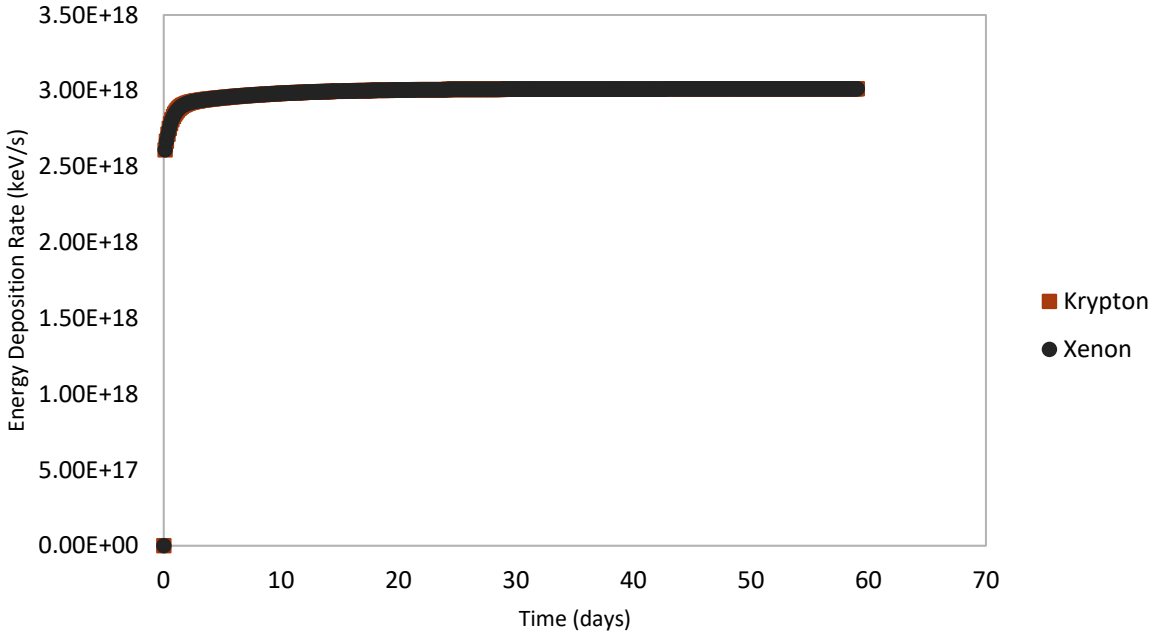

Figure 24. Energy deposition rate in the MOF trap from Kr and Xe.

Similarly, 5.56e-7 g/s krypton will be produced in the reactor and a 50 L tank of MOF will be able to capture 5.25 g of Krypton before breakthrough in 109.4 days. Using the same assumptions as Xe, the absorbed dose in this MOF tank due to beta particles from Krypton decay was calculated to be 132.7 Gy. These dose calculations can be used in future experiments to determine the stability of the MOF using an equivalent gamma dose.

3.0 Summary and Conclusions

This work explored metal organic frameworks as an alternate candidate material for noble gas management from LFTR off-gas at different temperatures. Several candidate MOF materials were downselected, including SBMOF-1, CuBTC, and UiO-66. All the MOFs were synthesized and characterized using XRD, BET, and SEM. Subsequently, all these sorbents were fabricated into engineered particles with and without polymers (PMMA and PAN). All the engineered particles were tested on a shaker table to demonstrate their mechanical stability. Samples of each type of engineered particles were exposed to Co-60 radiation. All the samples were characterized before and after radiation to demonstrate the radiation stability of these materials. Noble gas adsorption experiments were performed on MOF powder and composites at room temperature between 0 and 1 bar pressure.

Single column breakthrough experiments were performed using SBMOF-1 that had been pressed at 2k psi, and with PAN and PMMA composites, with simulated LFTR off-gas composition at different temperatures (1000ppmv Xe, 100ppmv Kr balanced with Ar). Xenon loading was optimized in terms of activation conditions, experimental temperature, flow rate, and gas composition. SBMOF-1 performance was directly compared with that of NUCON carbon. Based on our experiments to obtain the same performance as carbon in terms of Xe removal efficiency, the amount of SBMOF-1 required is 82% of that for NUCON carbon at 25°. At 0°C, the required amount is further decreased to 55% of NUCON carbon. For example, at 0°C, replacing NUCON carbon with SBMOF-1 would require using only 55 grams to every 100 grams of NUCON carbon. In addition to the reduction of mass, the packing density of SBMOF-1 (0.633 g/cc) is greater than that of NUCON carbon (0.55 g/cc), which would further reduce the volume of the column needed to do the separation. At 0°C, the greater efficiency and higher packing density of SBMOF-1 reduce the volume of the column to 48% of that needed if NUCON carbon were the sorbent.

4.0 Path Forward

Though the MOFs identified as part of this program look very promising, several areas need significant improvement and would benefit from the following:

- Develop a mechanically robust particle with minimal loss in capacity.
- Optimize the desorption temperatures.
- Test the effects of particle size and effect of relative humidity on noble gas adsorption
- Develop a radiation tolerant composite.
- Examine the effects of decay heat on MOF sorbent.
- Continue to improve the noble gas capacity and selectivity.
- Construct a bench-scale off-gas system and optimize SBMOF-1, then evaluate its performance in comparison with leading sorbent materials.

5.0 References

Banerjee, D., A. J. Cairns, J. Liu, R. K. Motkuri, S. K. Nune, C. A. Fernandez, R. Krishna, D. M. Strachan, and P. K. Thallapally. 2015. “Potential of Metal–Organic Frameworks for Separation of Xenon and Krypton.” *Accounts of Chemical Research* 48 (2): 211-219. https://doi.org/10.1021/ar5003126.

Banerjee, D., C. M. Simon, A. M. Plonka, R. K. Motkuri, J. Liu, X. Chen, B. Smit, J. B. Parise, M. Haranczyk, and P. K. Thallapally. 2016. “Metal–Organic Framework with Optimally Selective Xenon Adsorption and Separation.” *Nature Communications* 7 (1). https://doi.org/10.1038/ncomms11831. PMCID: PMC4909987.

Banerjee, D., Z. Zhang, A. M. Plonka, J. Li, and J. B. Parise. 2012. “A Calcium Coordination Framework Having Permanent Porosity and High Co2/N2 Selectivity.” *Crystal Growth & Design* 12 (5): 2162-2165. https://doi.org/10.1021/cg300274n.

Chui, S. S.-Y., S. M.-F. Lo, J. P. H. Charmant, A. G. Orpen, and I. D. Williams. 1999. “A Chemically Functionalizable Nanoporous Material $[Cu_3(Tma)_2(H_2o)_3]_N$.” *Science* 283 (5405): 1148-1150. https://doi.org/10.1126/science.283.5405.1148.

Elsaidi, S. K., M. H. Mohamed, A. S. Helal, M. Galanek, T. Pham, S. Suepaul, B. Space, D. Hopkinson, P. K. Thallapally, and J. Li. 2020a. “Radiation-Resistant Metal-Organic Framework Enables Efficient Separation of Krypton Fission Gas from Spent Nuclear Fuel.” *Nature Communications* 11 (1): 3103. https://doi.org/10.1038/s41467-020-16647-1.

Elsaidi, S. K., D. Ongari, M. H. Mohamed, W. Xu, R. K. Motkuri, M. Haranczyk, and P. K. Thallapally. 2020b. “Metal Organic Frameworks for Xenon Storage Applications.” *ACS Materials Letters* 2 (3): 233-238. https://doi.org/10.1021/acsmaterialslett.9b00468.

Liu, J., C. A. Fernandez, P. F. Martin, P. K. Thallapally, and D. M. Strachan. 2014. “A Two-Column Method for the Separation of Kr and Xe from Process Off-Gases.” *Industrial & Engineering Chemistry Research* 53 (32): 12893-12899. https://doi.org/10.1021/ie502156h.

Nichols, J. P., and F. T. Binford. 1971. *Status of Noble Gas Removal and Disposal.* United States. https://www.osti.gov/biblio/4684282.

Riley, B. J., S. Chong, W. Kuang, T. Varga, A. S. Helal, M. Galanek, J. Li, Z. J. Nelson, and P. K. Thallapally. 2020. “Metal–Organic Framework–Polyacrylonitrile Composite Beads for Xenon Capture.” *ACS Applied Materials & Interfaces* 12 (40): 45342-45350. https://doi.org/10.1021/acsami.0c13717.

Riley, B. J., J. McFarlane, G. D. DelCul, J. D. Vienna, C. I. Contescu, and C. W. Forsberg. 2019. “Molten Salt Reactor Waste and Effluent Management Strategies: A Review.” *Nuclear Engineering and Design* 345: 94-109. https://doi.org/10.1016/j.nucengdes.2019.02.002.

Salomon, W., C. Roch-Marchal, P. Mialane, P. Rouschmeyer, C. Serre, M. Haouas, F. Taulelle, S. Yang, L. Ruhlmann, and A. Dolbecq. 2015. “Immobilization of Polyoxometalates in the Zr-Based Metal Organic Framework Uio-67.” *Chemical Communications* 51 (14): 2972-2975. https://doi.org/10.1039/C4CC09986A.

Thallapally, P. K., Sinnwell, M. A., W. Kuang, and K. L. Simmons. 2019. *Develop Engineered Forms of MOF with Polymers.* Pacific Northwest National Laboratory PNNL-28497. Richland, WA. https://www.osti.gov/servlets/purl/1884322.

Welty, A. K., T. G. Garn, and M. Greenhalgh. 2018. *Initial Evaluation of Casdb MOF Xe and Kr Capacities.* NTRD-MRWFD-2018-000194 / INL/EXT-18-44890. Idaho Falls, ID: I. N. Laboratory. https://inldigitallibrary.inl.gov/sites/sti/sti/Sort_4887.pdf.

6.0 Appendix

Table A4. Complete SBMOF-1 Breakthrough Data Set Arranged by Column Packing

Material	Activation temperature (ºC)	Xe concentration (ppm)	Experiment temperature (ºC)	Flow rate (mL/min)	Capacity (mmol/kg)	Capacity at breakthrough point (mmol/kg)
SBMOF-1 2k psi	125	1000	25	10	75	42
SBMOF-1 2k psi	125	1000	25	15	75	39
SBMOF-1 2k psi	125	1300	0	10	N/A	211
SBMOF-1 2k psi	125	1000	0	15	N/A	166
SBMOF-1 2k psi	125	1300	-40	20	N/A	804
SBMOF-1 2k psi	100	1300	25	10	82	38
SBMOF-1 2k psi	100	1300	25	15	86	34

Table A5. SBMOF-1 10% PAN Breakthrough Results with Simulated LFTR off-gas

Material	Activation temperature (ºC)	Xe concen-tration (ppm)	Experi-ment. temp. (ºC)	Flow rate (mL/min)	Capacity (mmol/kg)	Capacity at breakthrough point (mmol/kg)
SBMOF-1 10% PAN	100	1000	25	15	21	1.56
SBMOF-1 10% PAN	100	1000	25	10	17	1.76
SBMOF-1 10% PAN	120	1000	25	10	27	3.41
SBMOF-1 10% PAN	150	1000	25	15	32	3.52
SBMOF-1 10% PAN	180	1000	25	10	31	3.53
SBMOF-1 10% PAN	180	1000	25	15	45	5.12
SBMOF-1 10% PAN	150	1000	0	15	61	5.31
SBMOF-1 10% PAN	150	1000	0	10	62	5.15
SBMOF-1 10% PAN	150	1000	-40	10	200	29.91
SBMOF-1 10% PAN	150	1000	-40	15	~200 (ran out of gas)	25.99

Table A6. SBMOF-1 10% PAN Breakthrough Results using Simulated Nuclear Reprocessing Plant Off-Gas

Material	Activation temperature (ºC)	Xe concen-tration. (ppm)	Experiment. temperature (ºC)	Flow rate (mL/min)	Capacity (mmol/kg)	Capacity at breakthrough point (mmol/kg)
SBMOF-1 10% PAN	150	1300	0	15	75	7.52
SBMOF-1 10% PAN	150	1300	0	10	66	7.31
SBMOF-1 10% PAN	150	1300	25	20	30	3.84
SBMOF-1 10% PAN	180	1300	25	10	29	3.65
SBMOF-1 10% PAN	180	1300	25	15	43	4.58

Pacific Northwest National Laboratory

902 Battelle Boulevard
P.O. Box 999
Richland, WA 99354
1-888-375-PNNL (7665)

www.pnnl.gov